First-principles thermal transport in amorphous Ge 2 Sb 2 Te 5 at the nanoscale

Thuy-Quynh Duong, Assil Bouzid, Carlo Massobrio, Guido Ori, Mauro Boero, Évelyne Martin

First-principles thermal transport in amorphous $Ge_2Sb_2Te_5$ at the nanoscale

Thuy-Quynh DUONG,[†] Assil BOUZID,[‡] Carlo MASSOBRIO,[¶] Guido ORI,[¶] Mauro BOERO,[¶] and Evelyne MARTIN[*,†,§]

[†]*Univ. Lille, CNRS, Centrale Lille, Yncréa ISEN, Univ. Polytechnique Hauts-de-France, UMR 8520 - IEMN, F-59000 Lille, France*

[‡]*Institut de Recherche sur les Céramiques, UMR 7315 CNRS - Université de Limoges, Centre Européen de la Céramique, 12 rue Atlantis, 87068 Limoges Cedex, France*

[¶]*Université de Strasbourg, CNRS, Institut de Physique et Chimie des Matériaux de Strasbourg, UMR 7504, Strasbourg F-67034, France*

[§]*Current address: Université de Strasbourg, CNRS, Laboratoire ICube, UMR 7357, F-67037 Strasbourg, France*

E-mail: evelyne.martin@unistra.fr

Abstract

Achieving a precise understanding of nanoscale thermal transport in phase change materials (PCMs), such as $Ge_2Sb_2Te_5$ (GST), is the key of thermal management in nanoelectronics, photonic and neuromorphic applications using non-volatile memories. By resorting to a first-principles approach to calculate the thermal conductivity of amorphous GST, we found that size effects and heat transport via propagative modes persist well beyond extended range order distances typical of disordered network-forming materials. Values obtained are in quantitative agreement with the experimental data, by revealing a strong size dependence of the thermal conductivity down to the 1.7-10 nm range, fully covering the scale of current PCMs-based devices. In particular, a reduction of thermal conductivity as large as 75% occurs for dimensions lying below 2 nm. These results provide a quantitative description of the thermal properties of amorphous GST at the nanoscale and are expected to underpin the development of PCMs-based device applications.

Graphical TOC Entry

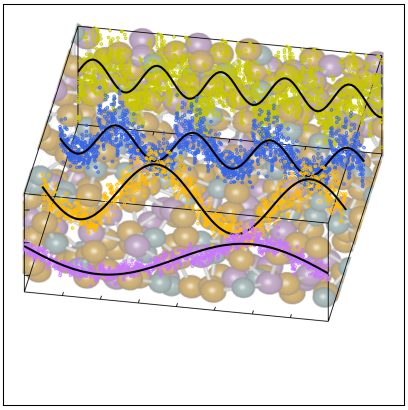

Keywords

Thermal conductivity, first-principles molecular dynamics, amorphous, phase-change materials

Computing with non-volatile memories (in-memory computing) is an efficient approach to reduce data transfer and optimize energy consumption within artificial intelligence schemes.[1] To this purpose, the technology based on phase-change materials (PCMs) proved worth pursuing.[2] PCMs are crucial for the development of emerging photonic and neuromorphic applications, ranging from non-volatile universal memory to optoelectronic systems suitable for nanophotonic devices and neuro-inspired computing.[3,4] Thermal management of PCMs enables the optimization of the supplied energy needed to switch between crystalline and amorphous states. At the memory cell level, low power operation calls for minimization of the current required to promote phase change (SET/RESET) via a comprehensive thermal design involving both PCM structural organizations. However, despite the considerable gain in knowledge of thermal transport in crystals, transport modes and size effects in disordered materials have escaped a quantitative assessment. To date, amorphous silicon is the only disordered material for which a reduction of thermal conductivity at short scale has been reported experimentally.[5] On the theoretical side, it appears that a depletion of thermal conductivity down to reduced dimensions could also occur in disordered chalcogenides.[6,7] Yet, it has to be established whether or not this behavior is general and holds for materials characterized by reversible structural changes between ordered and disordered phases. Interest in the ternary compound $Ge_2Sb_2Te_5$ (GST), a chalcogenide featuring prototypical properties for phase-change memories, stems from its high recrystallization speed as well as melting and glass transition points compatible with high data retention.[8–10] Thermal optimization of phase-change memories relies on the impact of nanoscale dimensions on the thermal conductivity κ. At the nanometer scale, a reduction of κ affects the operating of devices by slowing down heating and phase switching, with a direct consequence on the temporal response and energy consumption. This specific physical behavior requires reliable theoretical tools allowing for a quantitative description of thermal transport.

In the present work, we study the thermal conductivity of amorphous $Ge_2Sb_2Te_5$ (GST), investigate its dependence on size and quantify the short scale effects. We demonstrate that

a sizeable reduction of thermal conductivity can arise in PCMs at small sizes. To this end, we have resorted to first-principles molecular dynamics (FPMD) to generate the disordered structure and to the approach-to-equilibrium molecular dynamics (AEMD) strategy[11] to determine the thermal conductivity. We adopted the Car-Parrinello[12] framework as implemented in the CPMD code.[13] For the exchange-correlation part of the Kohn-Sham energy expression, we selected the exchange functional of Becke[14] and the correlation part of Lee, Yang and Parr[15] (BLYP). We described the valence-core interaction by norm-conserving pseudopotential as prescribed by Troullier-Martins.[16] Valence electrons are represented by a plane-wave basis set with a cutoff of 30 Ry, and expanded at the Γ point only. The fictitious electron mass was set to 500 a.u. and the time step to 5 a.u. to achieve optimal conservation of the constants of motion. The ionic temperature was controlled with a Nosé-Hoover[17–19] thermostat chain.[20] In Ref.[21] this scheme was employed for N=144 atoms (32 Ge, 32 Sb and 80 Te) in a cubic periodic simulation cell of side length 16.86 Å (model B hereafter). To assess the dependence of the thermal conductivity on the dimensions along and across the direction of thermal transport, we have created a new model D made of 252 atoms (56 Ge, 56 Sb and 140 Te) in a cubic simulation cell of 20.32 Å. Stable configurations were obtained from a canonical NVT (constant volume and temperature) trajectory with the following thermal cycle: T = 200 K (5 ps), 300 K (4 ps), 600 K (4 ps), 900 K (12 ps), 600 K (11 ps) and 300 K (15 ps). Then, model D was duplicated to obtain model D2, annealed for 5 ps at T =600 K and 5 ps at 300 K. In a further step, model D2 (N=504 atoms) was further duplicated to obtain model D4 (N=1008 atoms), this latter being annealed for 10 ps at T =300 K. Periodic boundary conditions are applied to D, D2 and D4. Cell dimensions of the four models are given in Table 1. We stress that our models have the dimensions of the most advanced nanometric phase-change memories.[22]

Our strategy featuring four distinct annealing and relaxation runs is intended to meet the requirement of models statistically uncorrelated while having in common, in the case of D, D2 and D4, the same original simulation box. The four models considered yield

Table 1: Our four models of amorphous GST. L is the supercell length in the heat transport direction and S is its cross section.

Name	N	S(Å^2)	L (Å)
B	144	16.86×16.86	16.86
D	252	20.32×20.32	20.32
D2	504	20.32×20.32	40.65
D4	1008	20.32×20.32	81.31

very close structural descriptions of amorphous GST in terms of comparison with available experimental quantities and characteristic motifs of the network. For instance, the total neutron structure factors $S_T(k)$ of models B, D, D2 and D4 are reported in Fig. 1 and compared with experiments.[23] They exhibit very similar patterns by substantiating the data

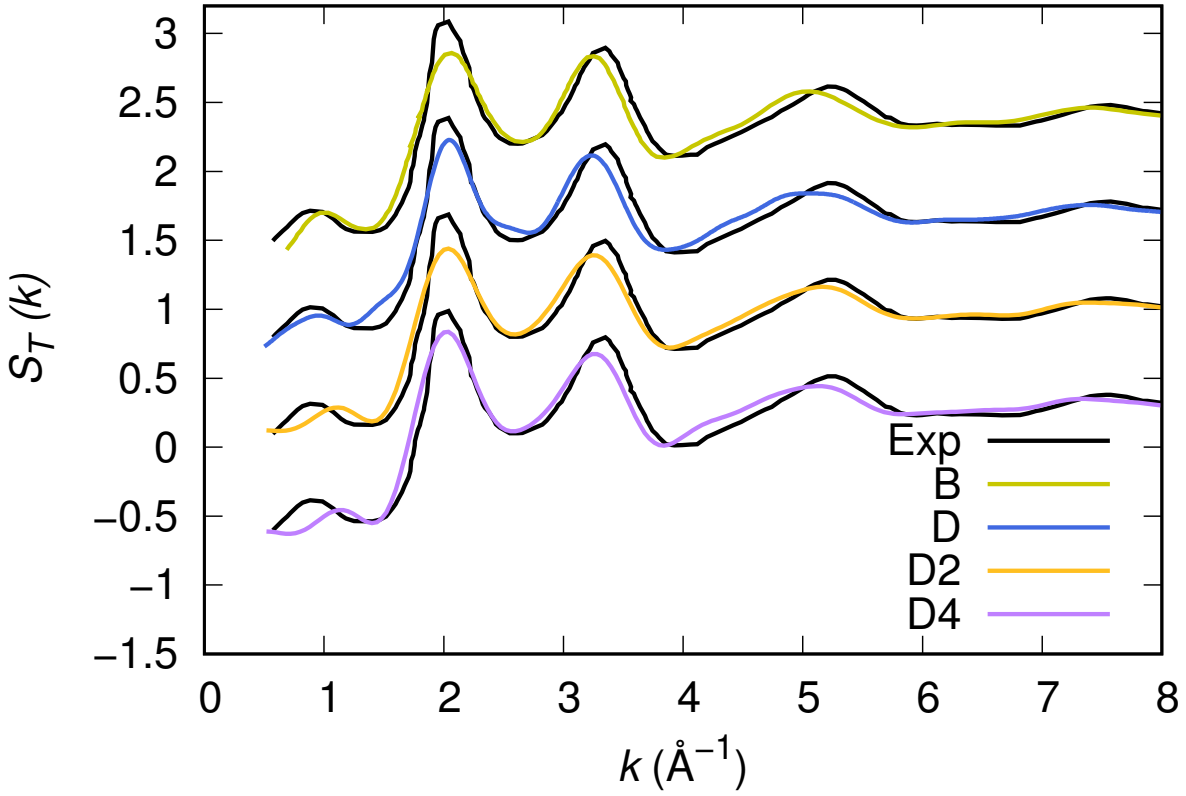

Figure 1: Experimental and calculated neutrons structure factor $S_T(k)$ of amorphous GST.

of Ref.[21] The intensities of all the peaks are well reproduced. Interestingly, $S_T(k)$ features a prominent bump at $k \approx 1$ Å^{-1}, indicative of intermediate range order extending up to

distances in the range 6-8 Å. Partial pair correlation functions are also very similar (see Fig. 2) as well as the coordination numbers n_{Ge}, n_{Sb}, n_{Te} for each species (Table 2). Small differences found among the four realizations have to be ascribed to statistical errors that are typically encountered when producing structures configurationally arrested over the time scales of molecular dynamics. The above pieces of evidence demonstrates unambiguously that the four samples of amorphous GST created by FPMD share the same essential topological features of the network, i.e. D, D2 and D4 do not introduce any relevant changes with respect to the description of Ref.[21] based on model B. Therefore, we can safely rule out the presence of size effects in the bulk properties of calculated amorphous GST. Stringent evidence on the predictive power of our FPMD approach for chalcogenides with models ranging in between $N{\approx}100$ and $N{\approx}500$ is summarized in Ref.[24]

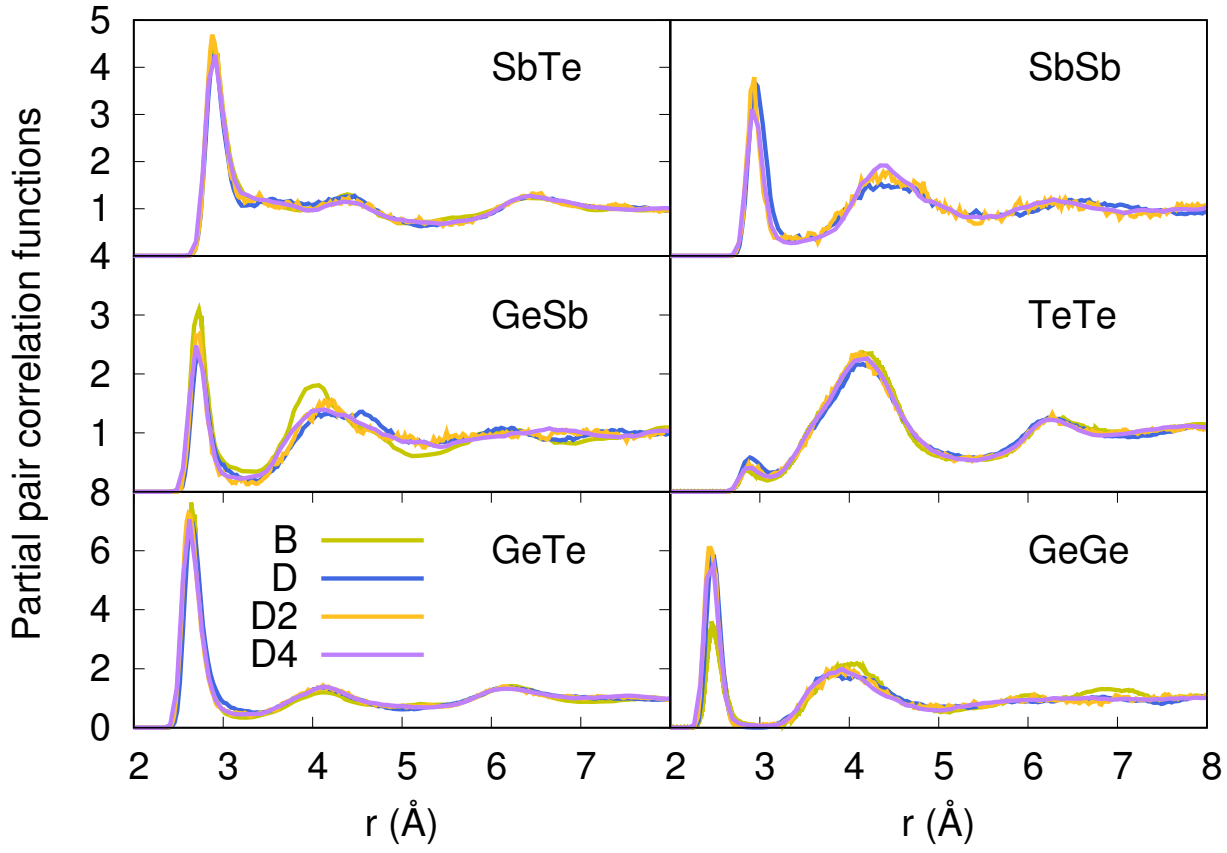

Figure 2: Partial pair correlation functions of the four models of amorphous GST

Within the AEMD method[11] we characterize a thermal process by relying on a thermal

Table 2: Coordination numbers for Ge (n_{Ge}), Sb (n_{Sb}) and Te (n_{Te}) in the four models.

Model	n_{Ge}	n_{Sb}	n_{Te}
B	4.03	3.99	2.58
D	4.13	3.81	2.66
D2	4.07	3.98	2.63
D4	3.98	4.03	2.63

transient and, in particular, its decay time τ, this methodology being well established as both effective and affordable.[6] The transient regime is obtained following two phases. During the first (phase 1), the system is divided in two blocks (see inset of Fig. 3). The hot block is kept at $T = 400$ K and the cold block at $T = 200$ K via two distinct thermostats maintained during 10 ps. At the end of phase 1, the temperature difference between the blocks is released, leading to a transient regime (phase 2) characterized by the decrease (increase) in temperature of the hot (cold) block. Fig. 3 shows the time evolution of the process for the largest model, D4.

Fig. 4 shows the temperature profiles in the four models averaged during the whole duration of phase 2. The profiles are sinusoidal with a period equal to the extension of the simulation cell along the transport direction (L). This proves that heat propagation occurs in the diffusive regime since the sine form is the solution of the heat equation in a one dimensional periodic system.

The decay time τ of the thermal transient observed during phase 2 of AEMD gives access to the thermal conductivity κ defined as:[25]

$$\kappa = \frac{L^2}{4\pi^2}\frac{C.\rho}{\tau}. \tag{1}$$

where C is the heat capacity calculated from the variation of the total energy versus temperature and ρ is the system density. Since the temperature difference $\Delta T(t)$ during phase 2 evolves to a very good extent according to an exponential decay, a decay time τ can be extracted for each model.

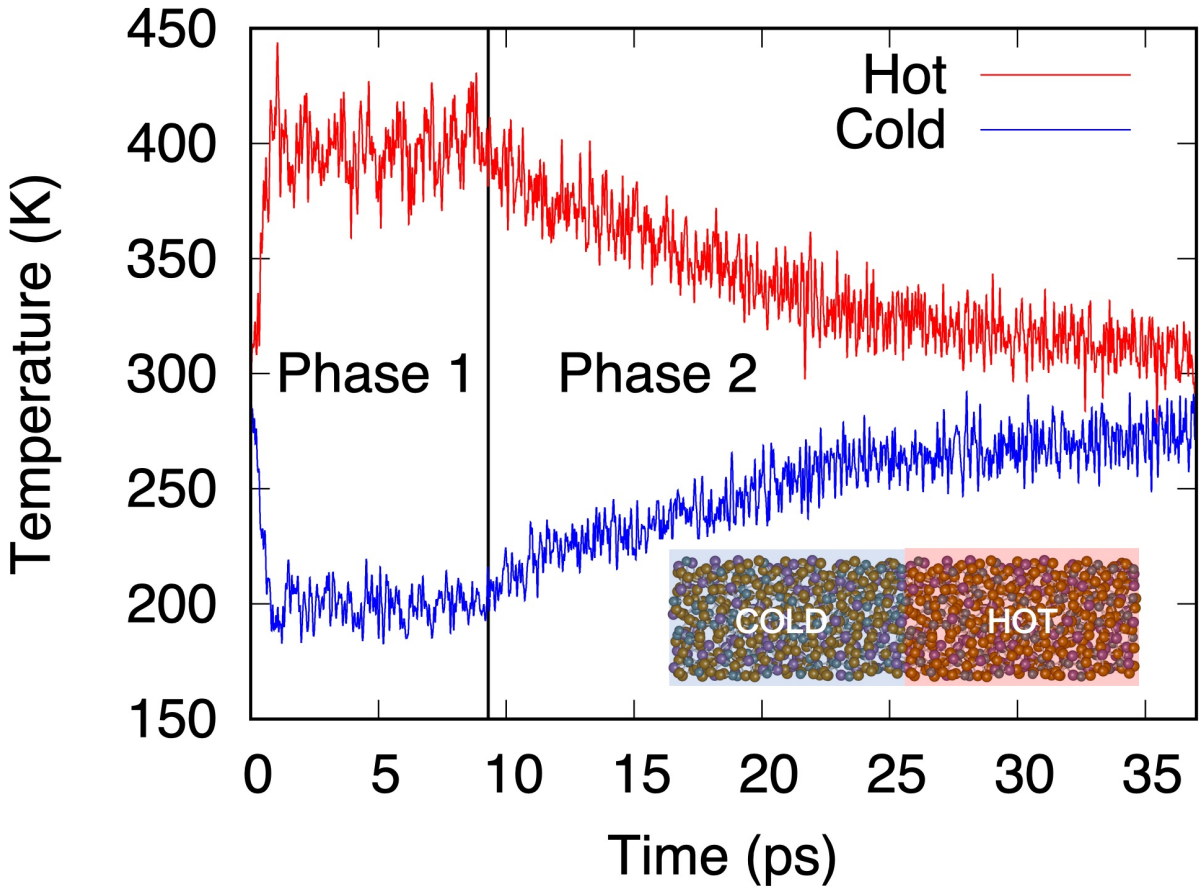

Figure 3: Temperatures in the hot (red line) and cold (blue line) blocks during the two phases of AEMD. Model D4 (N=1008 atoms) is presented in inset with the hot and cold blocks identified.

Thermal conductivities presented in Fig. 5 feature a dependence on the dimension of the simulation cell along the transport direction (L). This can be rationalized in terms of behavior of heat carriers. Heat carriers with mean free paths (MFP) smaller than L are those experiencing scattering events, while transport is ballistic for heat carriers with a higher MFP. When increasing L, the contribution of heat carriers of larger MFP increases until the bulk thermal conductivity is reached for L larger than the maximum MFP. For sizes larger than the maximum MFP, the thermal conductivity becomes independent on the system length.[26,27]

The evolution from a mixed ballistic-diffusive to a purely diffusive regime has been de-

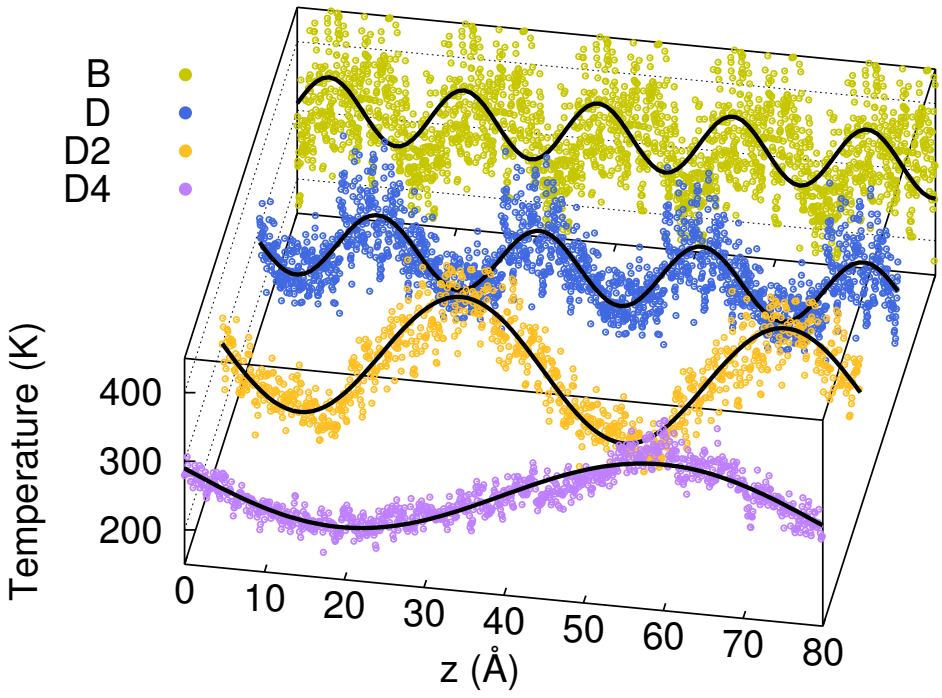

Figure 4: Temperature profiles in the four amorphous GST models during phase 2 of AEMD (dots). The data for the smallest models (B, D and D2) are replicated according to the peridodic boundary conditions. The lines are sine functions fitted to the AEMD data.

scribed analytically by Alvarez and Jou:[28]

$$\kappa_{\mathrm{AJ}}(L) = \kappa_{\mathrm{bulk}} \frac{L^2}{2\pi^2 l^2} \left[\sqrt{1 + 4\left(\frac{\pi l}{L}\right)^2} - 1 \right], \tag{2}$$

where κ_{bulk} is the bulk thermal conductivity and l is a parameter with the dimension of a length. Our results are consistent with Eq. 2, as shown in Fig. 5. The resulting bulk thermal conductivity κ_{bulk} equal to 0.26±0.04 W $\mathrm{K^{-1}m^{-1}}$ agrees with the experimental data reported in Table 3.

The existence of a length dependence in the heat transport direction means that propagative modes with a distribution of MFPs are responsible for heat transport in a way analogous

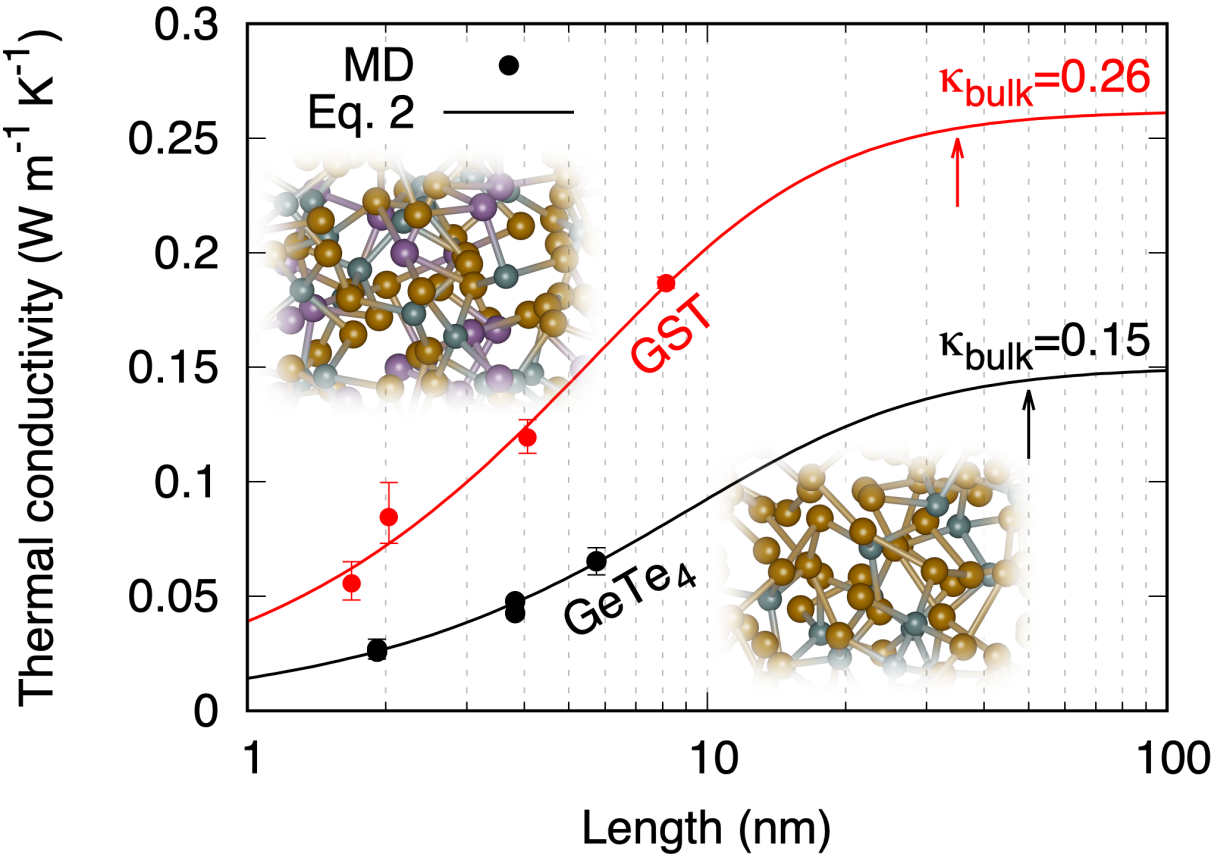

Figure 5: Thermal conductivities of amorphous GST calculated by AEMD (red dots). The results obtained in Ref.[6] for amorphous $GeTe_4$ using AEMD are also reported (black dots). The lines are fits following Alvarez and Jou's analytical model of size dependence (Eq. 2). The arrows indicate the maximum MFPs.

to phonons in crystals. In our FPMD-AEMD results the persistence of such length dependence up to 8 nm (size of model D4) cannot be related to enhanced structural order in the glass. In fact, such extended form of structural organization does exist in prototypical disordered AX_2 materials[36] but it does not extend to distances larger than 6 nm. At the largest sizes, a plateau occurs in the $\kappa(L)$ behavior for $L > 35$ nm (Fig. 5). Below this value, a sizeable reduction of thermal conductivity is detectable. It is instructive to consider the thermal conductivities of amorphous $GeTe_4$ as reported in Fig. 5, for which size effects persist up to even larger dimensions (≈ 50 nm).[6] Taken together, these findings prove that propagative modes and size effects are a general feature in chalcogenide glasses and have profound consequences in those prone to nanotechnology applications. This is illustrated in

Table 3: Experimental values of the thermal conductivity of amorphous GST (from top to bottom in chronological order).

Ref.	κ (W K^{-1}m^{-1})	Method	Dimensions (nm)
[29]	0.17	Laser-induced temperature distribution	20-85
[30]	0.24	3ω	98-200
[31]	0.24	3ω	300
[32]	0.19	Time-domain thermoreflectance	270
[33]	0.19	Photothermal radiometry	100-840
[34]	0.25±0.05	Time-domain thermoreflectance	30-150
[35]	0.30	Scanning thermal microscopy	100-200

Table 4 where we report the corresponding reductions of thermal conductivities at 10, 5 and 2 nm. The design of phase-change devices should therefore account for such a reduction of thermal conductivity at smaller technological nodes, that could lead to an increase of the switching time that would eclipse the benefits of downscaling.

Table 4: Reduction of thermal conductivity at short sizes.

	10 nm	5 nm	2 nm
GST	23%	46%	73%
$gGeTe_4$	38%	61%	82%

In conclusion, the thermal conductivity of amorphous $Ge_2Sb_2Te_5$ has been obtained within a first-principles methodology allowing for an affordable treatment of system sizes of about 1000 atoms and adequate simulation times. We obtained a quantitative agreement with experimental data, substantiated by a robust analytical extrapolation to macroscopic sizes. We found a length dependence of the thermal conductivity up to 35 nm, a clear indication that propagative carriers contribute to heat transport in spite of structural disorder. The reduction of the thermal conductivity manifests itself as a general feature in disordered chalcogenides, being quite significant (75%) in amorphous $Ge_2Sb_2Te_5$ for sizes below 2 nm, bearing an unavoidable impact on the thermal management of phase-change memories.

Acknowledgement

Sébastien Le Roux is acknowledged for constructive comments. Financial support of the French ANR via the project n. ANR-17-CE09-0039-02 “SIRENA" is gratefully acknowledged. Calculations were performed by using resources from GENCI (Grand Equipement National de Calcul Intensif) (Grants No. 0910296 and 095071).

References

(1) Ielmini, D.; Wong, H.-S. P. In-Memory Computing with Resistive Switching Devices. *Nature Electronics* **2018**, *1*, 333–343.

(2) Joshi, V.; Le Gallo, M.; Haefeli, S.; Boybat, I.; Nandakumar, S. R.; Piveteau, C.; Dazzi, M.; Rajendran, B.; Sebastian, A.; Eleftheriou, E. Accurate Deep Neural Network Inference Using Computational Phase-Change Memory. *Nature Communications* **2020**, *11*, 2473.

(3) Wuttig, M.; Bhaskaran, H.; Taubner, T. Phase-Change Materials for Non-Volatile Photonic Applications. *Nature Photonics* **2017**, *11*, 465.

(4) Zhang, W.; Mazzarello, R.; Wuttig, M.; Ma, E. Designing Crystallization in Phase-Change Materials for Universal Memory and Neuro-Inspired Computing. *Nature Reviews Materials* **2019**, *4*, 150–168.

(5) Wingert, M. C.; Zheng, J.; Kwon, S.; Chen, R. Thermal Transport in Amorphous Materials: A Review. *Semiconductor Science and Technology* **2016**, *31*, 113003.

(6) Duong, T.-Q.; Massobrio, C.; Ori, G.; Boero, M.; Martin, E. Thermal Conductivity and Transport Modes in Glassy $GeTe_4$ by First-Principles Molecular Dynamics. *Physical Review Materials* **2019**, *3*, 105401.

(7) Duong, T.-Q.; Massobrio, C.; Boero, M.; Ori, G.; Martin, E. Heat Transport in Disordered Network Forming Materials: Size Effects and Existence of Propagative Modes. *Computational Materials Science* **2020**, *177*, 109607.

(8) Wuttig, M.; Yamada, N. Phase-Change Materials for Rewriteable Data Storage. *Nature Materials* **2007**, *6*, 824–832.

(9) Burr, G. W.; Breitwisch, M. J.; Franceschini, M.; Garetto, D.; Gopalakrishnan, K.; Jackson, B.; Kurdi, B.; Lam, C.; Lastras, L. A.; Padilla, A. et al. Phase Change Memory Technology. *Journal of Vacuum Science & Technology B, Nanotechnology and Microelectronics: Materials, Processing, Measurement, and Phenomena* **2010**, *28*, 223.

(10) Noé, P.; Vallée, C.; Hippert, F.; Fillot, F.; Raty, J.-Y. Phase-Change Materials for Non-Volatile Memory Devices: From Technological Challenges to Materials Science Issues. *Semiconductor Science and Technology* **2017**, *33*, 013002.

(11) Lampin, E.; Palla, P. L.; Francioso, P.-A.; Cleri, F. Thermal Conductivity from Approach-to-Equilibrium Molecular Dynamics. *Journal of Applied Physics* **2013**, *114*, 033525.

(12) Car, R.; Parrinello, M. Unified Approach for Molecular Dynamics and Density-Functional Theory. *Physical Review Letters* **1985**, *55*, 2471–2474.

(13) Jointly by IBM Corporation and by Max Planck Institute, Stuttgart, CPMD code. 2019; `http://www.cpmd.org`.

(14) Becke, A. D. Density-Functional Exchange-Energy Approximation with Correct Asymptotic Behavior. *Physical Review A* **1988**, *38*, 3098–3100.

(15) Lee, C.; Yang, W.; Parr, R. G. Development of the Colle-Salvetti Correlation-Energy Formula into a Functional of the Electron Density. *Physical Review B* **1988**, *37*, 785–789.

(16) Troullier, N.; Martins, J. L. Efficient Pseudopotentials for Plane-Wave Calculations. *Physical Review B* **1991**, *43*, 1993–2006.

(17) Nosé, S. A Molecular Dynamics Method for Simulations in the Canonical Ensemble. *Molecular Physics* **1984**, *52*, 255–268.

(18) Nosé, S. A Unified Formulation of the Constant Temperature Molecular Dynamics Methods. *The Journal of Chemical Physics* **1984**, *81*, 511–519.

(19) Hoover, W. G. Canonical Dynamics: Equilibrium Phase-Space Distributions. *Physical Review A* **1985**, *31*, 1695–1697.

(20) Martyna, G. J.; Klein, M. L.; Tuckerman, M. Nosé–Hoover Chains: The Canonical Ensemble via Continuous Dynamics. *The Journal of Chemical Physics* **1992**, *97*, 2635–2643.

(21) Bouzid, A.; Ori, G.; Boero, M.; Lampin, E.; Massobrio, C. Atomic-Scale Structure of the Glassy $Ge_2Sb_2Te_5$ Phase Change Material: A Quantitative Assessment via First-Principles Molecular Dynamics. *Physical Review B* **2017**, *96*, 224204.

(22) Kersting, B.; Salinga, M. Exploiting Nanoscale Effects in Phase Change Memories. *Faraday Discussions* **2019**, *213*, 357–370.

(23) Jóvári, P.; Kaban, I.; Steiner, J.; Beuneu, B.; Schöps, A.; Webb, M. A. Local Order in Amorphous $Ge_2Sb_2Te_5$ and $GeSb_2Te_4$. *Physical Review B* **2008**, *77*, 035202.

(24) Bouzid, A.; Roux, S. L.; Ori, G.; Tugène, C.; Boero, M.; Massobrio, C. In *Molecular Dynamics Simulations of Disordered Materials: From Network Glasses to Phase-Change Memory Alloys*; Massobrio, C., Du, J., Bernasconi, M., Salmon, P. S., Eds.; Springer Series in Materials Science; Springer International Publishing: Cham, 2015; pp 313–344.

(25) Bouzid, A.; Zaoui, H.; Palla, P. L.; Ori, G.; Boero, M.; Massobrio, C.; Cleri, F.; Lampin, E. Thermal Conductivity of Glassy $GeTe_4$ by First-Principles Molecular Dynamics. *Physical Chemistry Chemical Physics* **2017**, *19*, 9729–9732.

(26) Zaoui, H.; Palla, P. L.; Cleri, F.; Lampin, E. Fourier-like Conduction and Finite One-Dimensional Thermal Conductivity in Long Silicon Nanowires by Approach-to-Equilibrium Molecular Dynamics. *Physical Review B* **2017**, *95*, 104309.

(27) Zaoui, H.; Palla, P. L.; Giordano, S.; Cleri, F.; Verdier, M.; Lacroix, D.; Robillard, J.-F.; Termentzidis, K.; Martin, E. Thermal Conductivity of Deca-Nanometric Patterned Si Membranes by Multiscale Simulations. *International Journal of Heat and Mass Transfer* **2018**, *126*, 830–835.

(28) Alvarez, F. X.; Jou, D. Memory and Nonlocal Effects in Heat Transport: From Diffusive to Ballistic Regimes. *Applied Physics Letters* **2007**, *90*, 083109.

(29) Peng, C.; Cheng, L.; Mansuripur, M. Experimental and Theoretical Investigations of Laser-Induced Crystallization and Amorphization in Phase-Change Optical Recording Media. *Journal of Applied Physics* **1997**, *82*, 4183–4191.

(30) Kim, E.-K.; Kwun, S.-I.; Lee, S.-M.; Seo, H.; Yoon, J.-G. Thermal Boundary Resistance at $Ge_2Sb_2Te_5$/ZnS:SiO_2 Interface. *Applied Physics Letters* **2000**, *76*, 3864–3866.

(31) Giraud, V.; Cluzel, J.; Sousa, V.; Jacquot, A.; Dauscher, A.; Lenoir, B.; Scherrer, H.; Romer, S. Thermal Characterization and Analysis of Phase Change Random Access Memory. *Journal of Applied Physics* **2005**, *98*, 013520.

(32) Lyeo, H.-K.; Cahill, D. G.; Lee, B.-S.; Abelson, J. R.; Kwon, M.-H.; Kim, K.-B.; Bishop, S. G.; Cheong, B.-k. Thermal Conductivity of Phase-Change Material $Ge_2Sb_2Te_5$. *Applied Physics Letters* **2006**, *89*, 151904.

(33) Battaglia, J.-L.; Kusiak, A.; Schick, V.; Cappella, A.; Wiemer, C.; Longo, M.; Varesi, E. Thermal Characterization of the SiO_2-$Ge_2Sb_2Te_5$ Interface from Room Temperature up to 400°C. *Journal of Applied Physics* **2010**, *107*, 044314.

(34) Lee, J.; Bozorg-Grayeli, E.; Kim, S.; Asheghi, M.; Philip Wong, H.-S.; Goodson, K. E. Phonon and Electron Transport through $Ge_2Sb_2Te_5$ Films and Interfaces Bounded by Metals. *Applied Physics Letters* **2013**, *102*, 191911.

(35) Bosse, J. L.; Timofeeva, M.; Tovee, P. D.; Robinson, B. J.; Huey, B. D.; Kolosov, O. V. Nanothermal Characterization of Amorphous and Crystalline Phases in Chalcogenide Thin Films with Scanning Thermal Microscopy. *Journal of Applied Physics* **2014**, *116*, 134904.

(36) Salmon, P. S.; Martin, R. A.; Mason, P. E.; Cuello, G. J. Topological versus Chemical Ordering in Network Glasses at Intermediate and Extended Length Scales. *Nature* **2005**, *435*, 75–78.